



Dendritic Silica@Aqueous Miscible Organic-Layered Double Hydroxide Hybrids

Hongri Suo†, Chunping Chen†, Jean-Charles Buffet, Dermot O'Hare

Received 00th January 20xx,
Accepted 00th January 20xx

DOI: 10.1039/x0xx00000x

www.rsc.org/

We present the synthesis of a series of hierarchical Silica@Layered Double Hydroxide (SiO₂@LDH) core@shell hybrid materials that have been post-treated using the Aqueous Miscible Organic Solvent Treatment (AMOST) method. The Silica@Aqueous Miscible Organic-Layered Double Hydroxide (SiO₂@AMO-LDH) hybrids exhibit composition flexibility with radially oriented hydrophobic AMO-Mg_yAl_{1-y}-CO₃-LDH nanosheets resulting in a new dendritic morphology.

Conventionally, layered double hydroxides (LDHs), a large family of anionic clays, can be commonly described by the general formula $[M^{2+}_{1-x}M'^{3+}_x(OH)_2](A^{n-})_{x/n} \cdot mH_2O$, where M, M' represent metal cations and A are anions.^{1, 2} Owing to their high positive surface charge, anion exchange capacity, and low cost; LDH are widely studied and used in the fields of heterogeneous catalysis, precursors to mixed oxides,^{3, 4, 5, 6-10} CO₂ adsorption,^{11, 12} ion exchange hosts,¹³⁻¹⁵ pharmaceutical delivery,^{4, 16-18} electrodes for biosensors and battery cathode precursors.¹⁹⁻²³ However, the LDHs synthesised by traditional co-precipitation methods normally exhibit stone-like morphologies because of the high degree of platelet aggregation by *ab*-face stacking during the drying process. This significantly limits their potentials and practical applications in catalysis and sorption chemistry. In 2013, O'Hare and co-authors developed a new generation of LDHs, named AMO-LDHs (AMO = aqueous miscible organic), in which the wet LDH cake is dispersed in an AMO solvent.^{24, 25} The AMO dispersion solvent (e.g. acetone, ethanol) can replace some of the water molecules bound on the surface or inside the layers; after drying these AMO-LDHs can form a highly dispersed flower-like morphology rather than the stone-like morphology typically observed for conventional LDHs (Fig. S1a). It was shown that this is an efficient method to

produce highly dispersed materials in solid phase with high surface area, pore volume and wide pore-size distributions.

Recently, core-shell nanocomposites have attracted increasing interest owing to their novel functionalities and synergetic properties.²⁶⁻²⁹ They also offer a low-cost synthetic strategy by coating expensive materials on an inexpensive core materials. There are increasing number of reports on core-shell LDH based nanocomposites. For example, Chen *et al.* have synthesised Fe₃O₄@LDH core-shell nanocomposites for wastewater treatment;³⁰ Wei and co-workers reported that LDH can grow on various templates *via* sol-gel nanocopying and *via in situ* growth processes³¹ and Zhang *et al.* have used coprecipitation methods to grow an LDH shell coating on magnesium ferrite core.^{32, 33} O'Hare group reported SiO₂@LDH and Zeolite@LDH core-shell nanocomposite synthesised by coprecipitation method.^{34, 35, 36}

In this study, we applied AMOST method to engineer the surface structure and properties of core-shell LDH materials, SiO₂@AMO-LDH, which have an outer shell coating of highly dispersed LDH platelets and inner core with monodispersed silica spheres (500 nm) (Fig. S2). The transmission electron microscope (TEM) images of water washed SiO₂@LDHs with various Mg/Al ratios (SiO₂@Mg_yAl_{1-y}-CO₃-LDH, *y* is the ratio of Mg/Al in LDH shell) are shown in Fig. 1a-c. It can be clearly observed that all samples with ratios from 2 to 4 exhibit typical core-shell structure where the dark core sphere was SiO₂ and hierarchical shell was LDH nanosheets which vertically grown on the SiO₂ surface. The thickness of the LDH shell increases from 110 to 269 nm with increasing *y* from 2 to 4. These results are in good agreement with the powder X-ray diffraction (XRD) patterns as shown in Fig. S3. All samples present a combination of the characteristic features of both silica (amorphous structure) and crystalline LDH (layer features). The crystallinity of LDH nanosheets increased with increasing Mg/Al ratios. SiO₂@LDH with the Mg/Al ratio of 4 presented larger LDH platelet, denser and thicker LDH shell and highest crystallinity.

Chemistry Research Laboratory, Department of Chemistry, University of Oxford, 12 Mansfield Road, Oxford, OX1 3TA, UK. E-mail: dermot.ohare@chem.ox.ac.uk; Tel: +44 (0)1865 272686

†Hongri Suo and Chunping Chen contribute equally to the project and are to be considered co-first authors.

Electronic Supplementary Information (ESI) available: [PXRD, TEM, ICP, TGA, CHN and BET]. See DOI: 10.1039/x0xx00000x

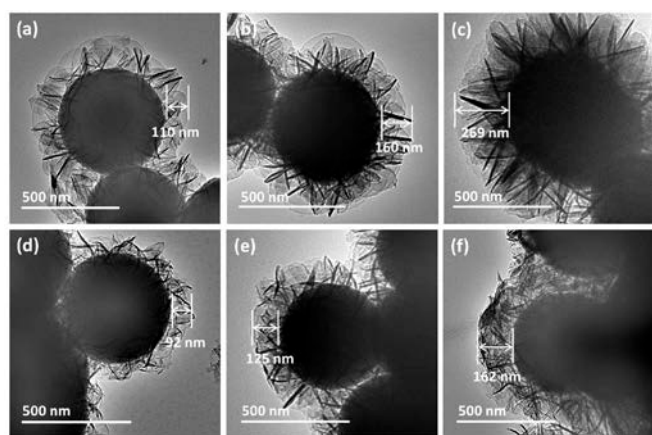


Fig. 1 TEM images of $\text{SiO}_2@\text{Mg}_4\text{Al-CO}_3\text{-LDH}$ prepared by in situ co-precipitation method with $y =$ (a) 2, (b) 3 and (c) 4; and $\text{SiO}_2@\text{AMO-LDH}$ dispersed in acetone for 20 h with $y =$ (d) 2, (e) 3 and (f) 4.

This is probably because 1) the lower amount of Al led to slower nuclear rate and larger LDH particle formation; 2) higher ratio of Mg/Al has lower positive charge density in the sample, which has lower coulombic repulsive force toward the new coming LDH precursors.

The AMOST method is an efficient method to produce highly dispersed microcrystalline LDH powders with high surface area. In this study, we found AMO solvent also played important role in core-shell LDH composites. As shown in Fig. 1d-f, morphology of LDH shell changed after AMOST post treatment with acetone. The thickness of LDH shell decreased from 110, 160, 269 nm to 92, 125 and 162 nm for $y = 2, 3$ and 4, respectively. We believe that may be due to the AMO solvent (*ie.* acetone) interrupting the hydrogen bonding network within LDH shell, leading to the formation of thinner LDH nanosheets and a curved LDH shell. Interestingly, varying the acetone dispersion time from 1, 4 to 20 h (using the same reaction conditions and Mg:Al ratio of 4) led to different LDH shell morphologies. As shown in Fig. 2, the AMO-LDH nanosheets became thinner and the edges bent after acetone treatment for 1 to 4 h. The thickness of LDH shell decreased from 242 to 201 nm but it remained platelet-like morphology. With longer dispersion time up to 20 h (Fig. 2c), the LDH platelets not only became thinner but also form a dendritic structure. The thickness of the LDH shell further decreases to 160 nm. The greater exfoliation of the thinner LDH nanosheets by the AMO solvent leads to formation of a branch-like morphology for the LDH shell. Importantly, this core-shell morphology could be retained even after calcination at 400 °C for 6 h (Fig. S4). The AMO-LDO platelets became thinner but were still covalently bonded to the surface of the silica core via Al–O–Si covalent linkages.¹⁹ Interestingly, after rehydration in sodium carbonate solution, the LDO nanosheets regenerate/reconstruct to crystalline LDHs vertically aligned on the silica surface.

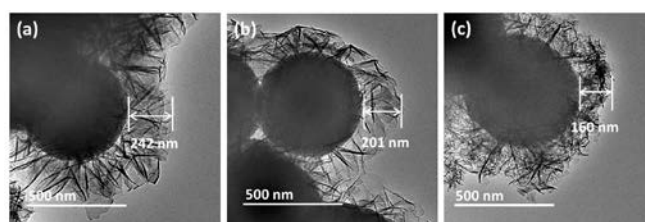


Fig. 2 TEM images of $\text{SiO}_2@\text{AMO-Mg}_4\text{Al-CO}_3\text{-LDH}$ with the different dispersion time in acetone (a) 1 h, (b) 4 h and (c) 20 h.

The N_2 adsorption and desorption isotherms of $\text{SiO}_2@\text{Mg}_4\text{Al-CO}_3\text{-LDHs}$ are shown in Fig. S5. According to the IUPAC classification, all samples exhibited type IV isotherm and H3 hysteresis loop, indicating that those were formed of typical plate-like particles with slit-shape pores. The specific BET surface areas and pore volumes of the samples before and after AMOST treatment are shown in Fig. 3a. It can be easily found that the samples after AMOST treatment showed much higher specific BET surface area and larger pore volumes compared with the sample without AMOST. The specific BET surface area gradually increased from 52 to 144 $\text{m}^2 \text{g}^{-1}$ with increasing acetone dispersion time from 0 to 20 h. The corresponding pore volumes also showed similar trend as that of BET surface area (Fig. 3a). The pore volumes increased from 0.35 to 0.60 cm^3/g when acetone dispersion time increased from 1 to 20 h. This is consistent with the observation from the TEM images (Fig. 2) which showed that the LDH nanosheets became thinner and moved towards branch-like morphology with increased acetone dispersion time. It is worth noting that the specific surface area of core material (SiO_2) is very low (17 m^2/g), and it remains the same even after AMOST treatment by acetone for 20 h. These findings indicated that the AMO solvent (acetone) could effectively increase specific BET surface areas and pore volumes by interacting with the LDH shell rather than SiO_2 core, producing a dendritic shell. Therefore, it is not surprising to find that the bulk and tap density (Fig. S6) of $\text{SiO}_2@\text{AMO-Mg}_4\text{Al-CO}_3\text{-LDHs}$ are much lower than those of $\text{SiO}_2@\text{Mg}_4\text{Al-CO}_3\text{-LDHs}$. The detailed effect of acetone on the porosity and pore size distribution of $\text{SiO}_2@\text{Mg}_4\text{Al-CO}_3\text{-LDH}$ is shown in Fig. 3b. The sample without AMOST treatment does not possess any pore structure (dense stone-like powder after drying).³⁷ After 1 h of acetone dispersion, two additional pore distributions can be observed in the range of 5 – 18 and 20 – 40 nm. Interestingly, the pores in the range of 5 – 18 nm shifted to larger pore size range after 20 h of acetone dispersion. The longer dispersion time resulted in further exfoliation of the LDH nanosheets. The crystalline structure and phase purity of $\text{SiO}_2@\text{AMO-Mg}_4\text{Al-CO}_3\text{-LDHs}$ with various acetone dispersion time were examined by powder X-ray crystallography (PXRD) and solid-state ^{27}Al nuclear magnetic resonance (^{27}Al SSNMR).

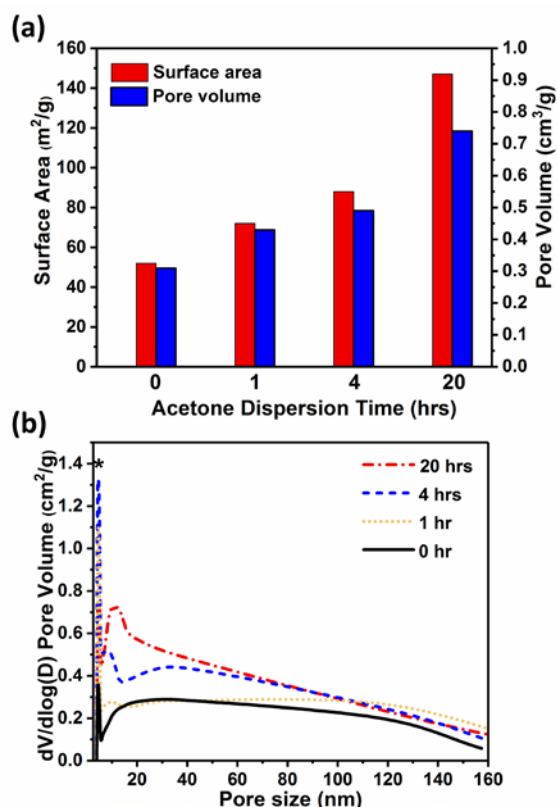


Fig. 3 (a) Specific BET surface areas and pore volume and (b) pore size distribution of $\text{SiO}_2@\text{Mg}_4\text{Al-CO}_3\text{-LDH}$ with AMOST post treatment in acetone for 0, 1, 4 and 20 h.

As shown in Fig. S7, all samples showed similar XRD patterns to that of $\text{SiO}_2@\text{Mg}_4\text{Al-CO}_3\text{-LDH}$ s, indicating that the crystal structure of the bulk material is not affected by the AMOST treatment. However, by measuring the Bragg reflections peak widths we noted that the crystalline domain length (CDL) computed by the Scherrer equation in the *c*-axis direction (Table S1) decreased with increasing AMO solvent dispersion time. This could be due to partial exfoliation of the LDH nanosheets; which is supported by TEM observations (Fig. 2) and previous literature reports.^{25,37} However, longer AMOST treatment times (20 h) leads to small amount of leaching of aluminium from LDH layers to form a disordered phase and the generation of some tetrahedral Al sites. The solid ^{27}Al NMR of $\text{SiO}_2@\text{Mg}_4\text{Al-CO}_3\text{-LDH}$ (Fig. S8) exhibits a dominant intensity resonance at -17 ppm and much smaller intensity resonances between *ca.* 30 – 50 ppm, which are assigned to the resonances of octahedral Al in the LDH layers and tetrahedral Al sites containing Si-O-Al linkages respectively. The resonances corresponding to the tetrahedral Al sites only appear after AMOST treatment and become more intense after 20 h, when multiple resonances can be resolved in the 30 – 50 ppm range.

The elemental composition of the obtained samples were analysed using thermogravimetric analysis (TGA), inductively coupled plasma mass spectrometry (ICP-MS) and elemental microanalysis (CHN). The results were summarised in Table S2. The mole ratio of SiO_2 and LDH in the samples was found to be 1.86. Hence, the final formulation of $\text{SiO}_2@\text{Mg}_4\text{Al-CO}_3\text{-LDH}$ s and $\text{SiO}_2@\text{AMO-Mg}_4\text{Al-CO}_3\text{-LDH}$ s after 20 h of AMOST treatment

can be defined as $[\text{SiO}_2]_{0.65} @ [\text{Mg}_{3.3}\text{Al}(\text{OH})_{8.6}(\text{CO}_3)_{0.5}(\text{H}_2\text{O})_{1.3}]_{0.35}$ and $[\text{SiO}_2]_{0.65} @ [\text{Mg}_{3.2}\text{Al}(\text{OH})_{8.4}(\text{CO}_3)_{0.5}(\text{H}_2\text{O})_{0.2}(\text{C}_3\text{H}_6\text{O})_{0.01}]_{0.35}$, respectively.

We were particularly interested in studying the basicity/acidity properties of these hybrid materials in order to probe their potential in catalysis. The temperature-programmed desorption of carbon dioxide (TPD- CO_2) was used to identify the basicity for these core-shell materials after calcination of 550°C for 3 h. One unanticipated finding was that the total amount of evolved CO_2 decreased from 2.58 to 1.01 mmol- CO_2/g with increasing acetone dispersion time from 0 to 20 h (Table S3). The $\text{SiO}_2@\text{AMO-Mg}_4\text{Al-CO}_3\text{-LDH}$ s after 20 h of AMOST showed the lowest basicity value, though it has the highest specific surface area. Furthermore, the strength of the basic sites decreased after AMOST method (Fig. S9). The same trend was also found for $\text{AMO-Mg}_4\text{Al-CO}_3\text{-LDH}$ s without a core material (Fig. S10 and Table S3). We postulate that some adsorbed acetone may thermally decompose during the calcination process, leading to blocking of the basic sites or alternatively some acetone self-condensation catalysed by the LDH may occur during the AMOST treatment or calcination process. The products from these reactions may then block some of the basic sites. Self-condensation reactions using LDH/LDO catalysis have also been reported^{38–40}. Further efforts are ongoing to explore and fully understand the effects of AMO solvent dispersions on the basic properties of these materials.

We find that AMOST treatment plays a key role in engineering the morphology and surface chemistry of core-shell LDH hybrids nanocomposites. During the AMOST process, AMO solvent replaces the surface bound water from the primary LDH particles and so rendering them organophilic rather than hydrophilic. These particles then have a much-diminished driving force for *ab*-face aggregation, leading to the formation of well-dispersed LDH nanosheets and a dendritic shell with high specific surface area as shown in Fig. 4. Longer AMO solvent dispersion time (> 20 h) results in partial leaking of aluminium.

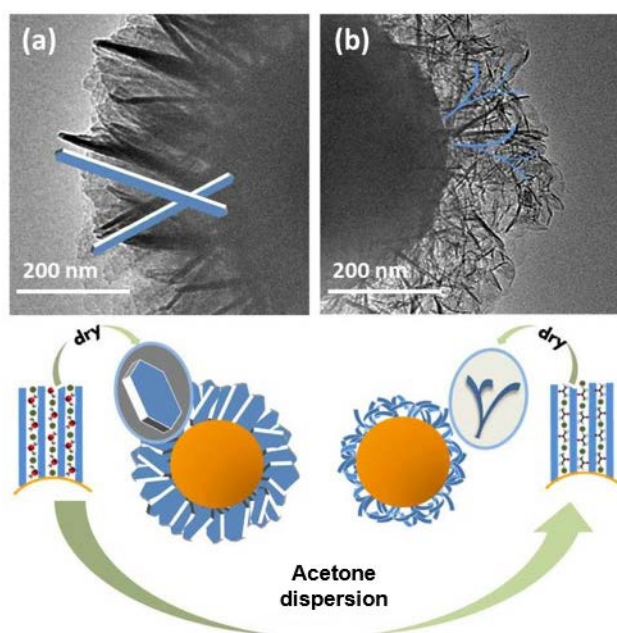


Fig. 4 TEM images of a) SiO₂@Mg₃Al-CO₃-LDH and b) SiO₂@AMO-Mg₃Al-CO₃-LDH after 20 h dispersion in acetone. Below is schematic representation of core@shell morphology.

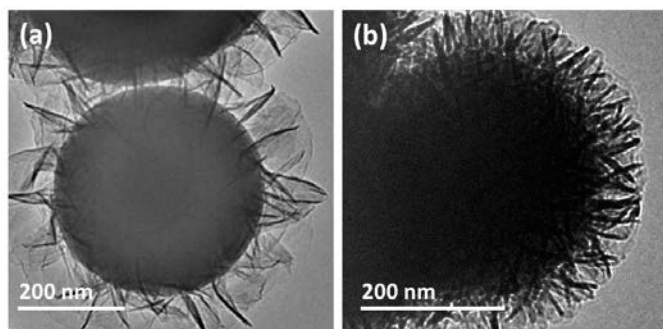


Fig. 5 TEM images of SiO₂@AMO-Mg₃Al_{0.4}Fe_{0.6}-CO₃-LDH and SiO₂@AMO-Mg_{3.2}Al₁Ni_{1.8}-CO₃-LDH after dispersion in acetone for 4 h.

We have expanded this methodology to other LDHs, synthesising a sunflower-like morphology for SiO₂@AMO-Mg₃Al_{1-z}Fe_z-CO₃ and a daisy-like morphology for SiO₂@AMO-Mg_{3-z}Al₁Ni_z-CO₃ (Fig. 5 and S11). The same effects on the platelets was observed after AMOST treatment using ethanol (Fig. S12). However, AMOST using ethanol dispersion seemed to have a milder effect on the materials as compared with acetone. Overall, the size of LDH platelets and the AMO solvent dispersion time are the primary factors controlling the synthesis of SiO₂@AMO-LDH.

In conclusion, we have developed further insights into the role of the AMO solvent dispersion in preparing SiO₂@AMO-LDH core@shell hybrids. Our method combines the advantages of a 3D hierarchical (SiO₂@LDH) and the surface properties of AMO-LDHs. SiO₂@AMO-LDHs exhibit thinner and more distorted LDH nanosheets affording a new dendritic morphology. The surface basicity of the SiO₂@AMO-LDHs can be modified by using various AMO solvents. The structural

stability of this SiO₂@AMO-LDH core-shell materials are promising candidates for use in catalysis.

H.S., C.C., J.-C.B. would like to thank SCG Chemicals Co., Ltd. (Thailand) for funding and Dr Nicholas H. Rees (University of Oxford) for solid state NMR spectroscopy analysis.

There are no conflicts of interest to declare.

Notes and references

1. F. T. F. Cavani, A. Vaccari, *Catal. Today*, 1991, **11**, 173-301.
2. X. Duan and D. G. Evans, *Layered double hydroxides*, Springer Science & Business Media, 2006.
3. J. L. Feng Li, D. G. Evans and X. Duan, *Chem. Mater.*, 2004, **16**, 1597-1602.
4. B. Li, J. He, D. G. Evans and X. Duan, *Appl. Clay. Sci.*, 2004, **27**, 199-207.
5. C. Qi, J. C. Amphlett and B. A. Peppley, *Appl. Catal., A*, 2006, **302**, 237-243.
6. X. Xu, R. Lu, X. Zhao, S. Xu, X. Lei, F. Zhang and D. G. Evans, *Appl. Catal., B*, 2011, **102**, 147-156.
7. Y. S. H. Morioka, M. Sukenobu, K. Ito, E. Tanabe, T. Shishido and K. Takehira, *Appl. Catal., A*, 2001, **215**, 11-19.
8. J. I. Di Cosimo, V. K. Díez, M. Xu, E. Iglesia and C. R. Apesteguía, *J. Catal.*, 1998, **178**, 499-510.
9. L. He, Y. Huang, A. Wang, Y. Liu, X. Liu, X. Chen, J. J. Delgado, X. Wang and T. Zhang, *J. Catal.*, 2013, **298**, 1-9.
10. S. Abello, D. Verboekend, B. Bridier and J. Perezramirez, *J. Catal.*, 2008, **259**, 85-95.
11. A. Garcia-Gallastegui, D. Iruretagoyena, V. Gouvea, M. Mokhtar, A. M. Asiri, S. N. Basahel, S. A. Al-Thabaiti, A. O. Alyoubi, D. Chadwick and M. S. P. Shaffer, *Chem. Mater.*, 2012, **24**, 4531-4539.
12. Q. Wang, H. H. Tay, Z. Zhong, J. Luo and A. Borgna, *Energ. Environ. Sci.*, 2012, **5**, 7526.
13. W. J. I. and C. Chisem, *J. Mater. Chem.*, 1994, **4**, 1737-1744.
14. A. M. Fogg, J. S. Dunn, S.-G. Shyu, D. R. Cary and D. O'Hare, *Chem. Mater.*, 1998, **10**, 351-355.
15. F. Millange, R. I. Walton, L. Lei and D. O'Hare, *Chem. Mater.*, 2000, **12**, 1990-1994.
16. A. C. S. Alcântara, P. Aranda, M. Darder and E. Ruiz-Hitzky, *J. Mater. Chem.*, 2010, **20**, 9495.
17. M. del Arco, S. Gutiérrez, C. Martín, V. Rives and J. Rocha, *J. Solid State Chem.*, 2004, **177**, 3954-3962.
18. S. Guan, R. Liang, C. Li, D. Yan, M. Wei, D. G. Evans and X. Duan, *J. Mater. Chem. B*, 2016, **4**, 1331-1336.
19. D. Shan, W. Yao and H. Xue, *Electroanalysis*, 2006, **18**, 1485-1491.
20. Z.-A. Hu, Y.-L. Xie, Y.-X. Wang, H.-Y. Wu, Y.-Y. Yang and Z.-Y. Zhang, *Electrochim. Acta*, 2009, **54**, 2737-2741.
21. C. M. Dan Shan, and Serge Cosnier, *Anal. Chem.*, 2004, **76**, 178-183.
22. M. Shao, F. Ning, Y. Zhao, J. Zhao, M. Wei, D. G. Evans and X. Duan, *Chem. Mater.*, 2012, **24**, 1192-1197.
23. M. Shao, R. Zhang, Z. Li, M. Wei, D. G. Evans and X. Duan, *Chem. Commun.*, 2015, **51**, 15880-15893.

24. Q. Wang and D. O'Hare, *Chem. Commun.* 2013, **49**, 6301-6303.
25. C. Chen, M. Yang, Q. Wang, J.-C. Buffet and D. O'Hare, *J. Mater. Chem., A*, 2014, **2**, 15102.
26. S. Kim, B. Fisher, H.-J. Eisler and M. Bawendi, *J. Am. Chem. Soc.*, 2003, **125**, 11466-11467.
27. E. Hofman, R. J. Robinson, Z.-J. Li, B. Dzikovski and W. Zheng, *J. Am. Chem. Soc.*, 2017, **139**, 8878-8885.
28. C. Würth, S. Fischer, B. Grauel, A. P. Alivisatos and U. Resch-Genger, *J. Am. Chem. Soc.*, 2018, **140**, 4922-4928.
29. M. Shao, F. Ning, J. Zhao, M. Wei, D. G. Evans and X. Duan, *J. Am. Chem. Soc.*, 2012, **134**, 1071-1077.
30. F. Mi, X. Chen, Y. Ma, S. Yin, F. Yuan and H. Zhang, *Chem. Commun* 2011, **47**, 12804-12806.
31. Y. Zhao, S. He, M. Wei, D. G. Evans and X. Duan, *Chem. Commun.*, 2010, **46**, 3031-3033.
32. H. Zhang, D. Pan, K. Zou, J. He and X. Duan, *J. Mater. Chem.*, 2009, **19**, 3069.
33. D. P. Hui Zhang, and Xue Duan, *J. Phys. Chem. C*, 2009, **113**, 12140-12148.
34. C. Chen, R. Felton, J.-C. Buffet and D. O'Hare, *Chem. Commun.*, 2015, **51**, 3462-3465.
35. J.-C. Buffet, C. F. Byles, R. Felton, C. Chen and D. O'Hare, *Chem. Commun.*, 2016, **52**, 4076-4079.
36. C. Chen, C. F. H. Byles, J.-C. Buffet, N. H. Rees, Y. Wu and D. O'Hare, *Chem. Sci.*, 2016, **7**, 1457-1461.
37. C. Chen, A. Wangriya, J.-C. Buffet and D. O'Hare, *Dalton Trans.*, 2015, **44**, 16392-16398.
38. D. Tichit, M. N. Bennani, F. Figueras, R. Tessier, *App. Clay Sci.*, 1998, **13**, 401.
39. P. Kuśtrowski, D. Sułkowska, L. Chmielarz, A. Rafalska-asocha, Dudek B, Dziembaj R. *Micropor. and Mesopor. Mater.* 2005, **78**, 11.
40. F. Prinetto, D. Tichit, R. Teissier, B. Coq. *Catal. today*. 2000, **55**, 103.